Supplementary Information for: Model-based characterization of the equilibrium dynamics of transcription initiation and promoter-proximal pausing in human cells

Yixin Zhao[1], Lingjie Liu[1,2], and Adam Siepel[1,2,*]

[1]Simons Center for Quantitative Biology, Cold Spring Harbor Laboratory, Cold Spring Harbor, NY
[2]Graduate Program in Genetics, Stony Brook University, Stony Brook, NY
[*]Corresponding author: asiepel@cshl.edu

Supplementary Table

symbol	parameter	values
α	Potential initiation rate (relative)	$\alpha\zeta$ = 0.1, 1, 10 events/min.
β	Pause escape rate (relative)	$\beta\zeta$ = 0.1, 1, 10 events/min.
ζ	Elongation rate	Mean = 2,000 bp/min. SD = 1,000 bp/min. Max = 2,500 bp/min. Min = 1,500 bp/min.
k	Position of the pause site (fixed)	50 bp downstream of TSS
	Position of the pause site (variable)	Mean = 50 bp SD = 25 bp Max = 17 bp Min = 200 bp
s_p	RNAP center-to-center spacing	33, 50, 70 bp
Δt	Time slice	10^{-4} min.
T	Total time	40 min.
C	Total cells simulated	20,000 cells
N	Total length of the simulated gene	2,000 bp in simulation 20,000 bp in Poisson sampling

Supplementary Table S1: Summary of parameters and the corresponding values used in simulation

Supplementary Figures

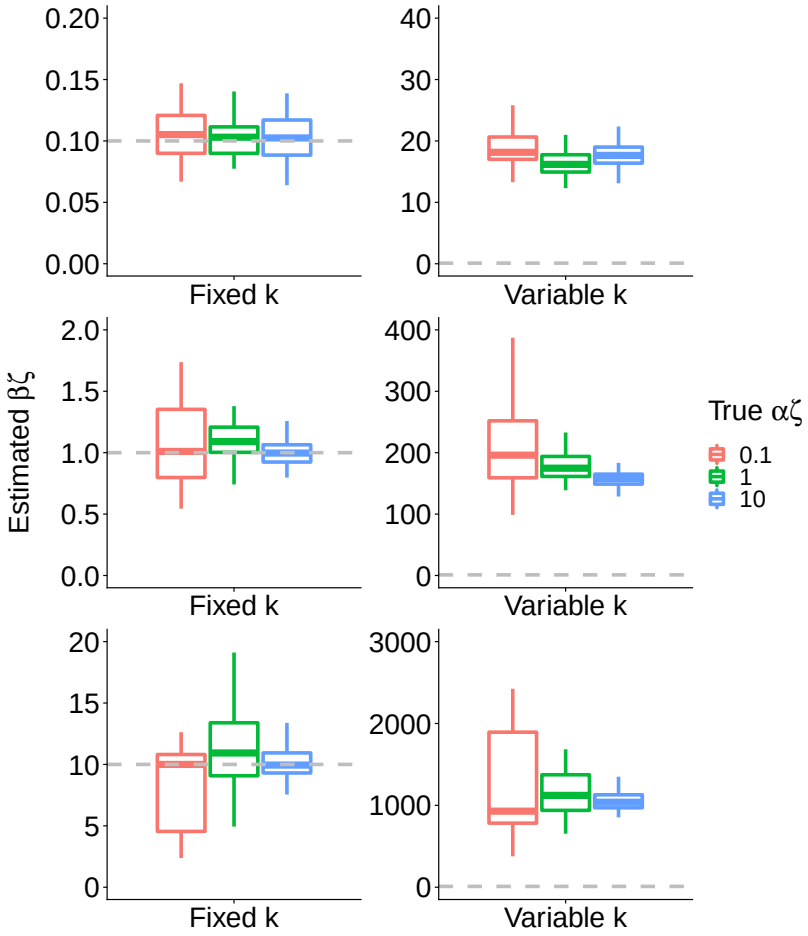

Supplementary Figure S1: Estimated values of $\beta\zeta$ under the initial model for simulated true values of $\beta\zeta \in \{0.1, 1.0, 10\}$ (top to bottom) and $\alpha\zeta \in \{0.1, 1, 10\}$ (see key), when the pause-site k is fixed (left) or variable across cells (right) in simulation. This is an expanded version of **Fig. 2B** showing a broader range of $\beta\zeta$ values. As in that case, dashed lines indicate the ground truth; boxplots summarize 50 replicates of the simulation; box boundaries indicate 1st and 3rd quartiles, and horizontal line indicates median. A value of $\zeta = 2$ kb/min is assumed so that $\alpha\zeta$ and $\beta\zeta$ can be assumed to have units of events per minute. Pause sites occur at a mean position of $k = 50$ bp. In the variable case, we assume a Gaussian distribution with a standard deviation of 25 bp.

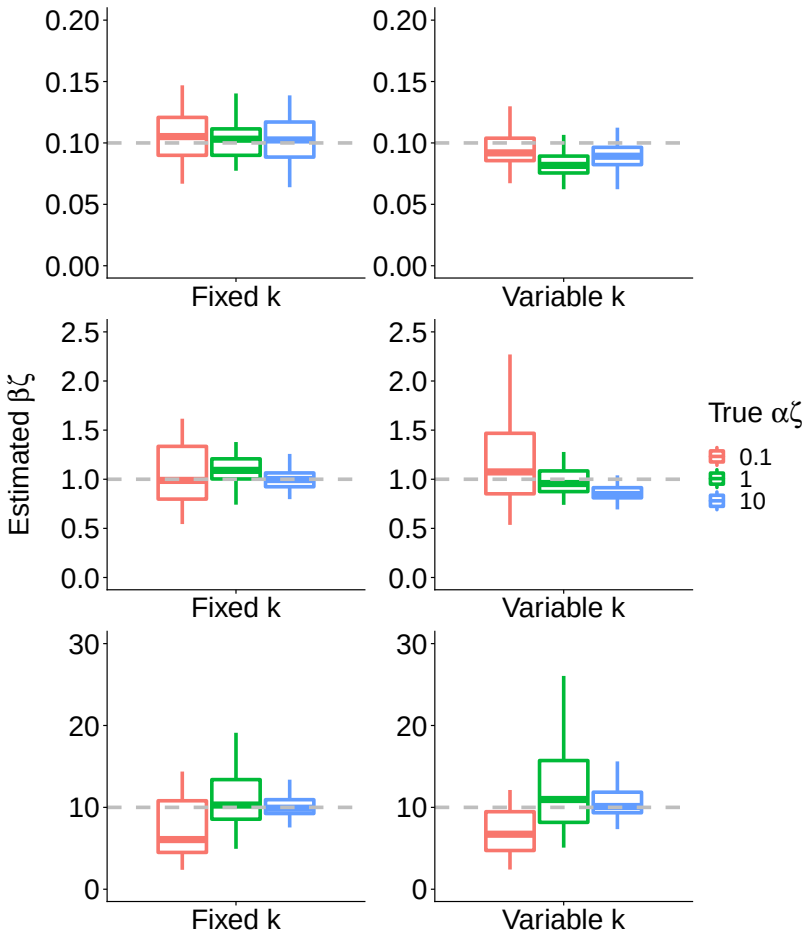

Supplementary Figure S2: Estimated values of $\beta\zeta$ under the variable-pause-site model for simulated true values of $\beta\zeta \in \{0.1, 1.0, 10\}$ (top to bottom) and $\alpha\zeta \in \{0.1, 1, 10\}$ (see key), when the pause-site k is fixed (left) or variable across cells (right) in simulation. This is an expanded version of **Fig. 3A** showing a broader range of $\beta\zeta$ values. As in that case, dashed lines indicate the ground truth; boxplots summarize 50 replicates of the simulation; box boundaries indicate 1st and 3rd quartiles, and horizontal line indicates median. A value of $\zeta = 2$ kb/min is assumed so that $\alpha\zeta$ and $\beta\zeta$ can be assumed to have units of events per minute. Pause sites occur at a mean position of $k = 50$ bp. In the variable case, we assume a Gaussian distribution with a standard deviation of 25 bp.

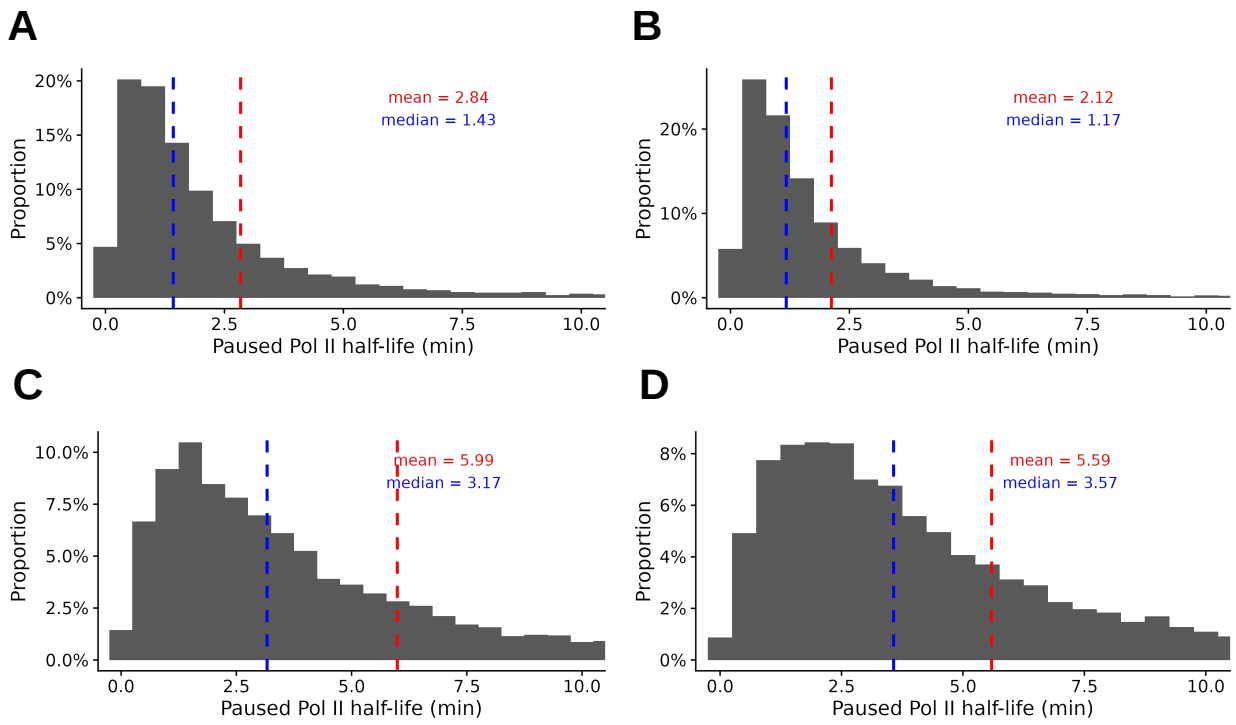

Supplementary Figure S3: Distributions of half-lives for paused RNAPs for (A) the untreated K562 cells from Vihervaara et al. [1], (B) the untreated K562 cells from Dukler et al. [2], (C) the heat-shock-treated K562 cells from Vihervaara et al. [1], and (D) the celastrol-treated (160-min) K562 cells from Dukler et al. [2]. The histograms are truncated at 10 min. for clarity. See **Methods** for details on the calculation of half-lives from β estimates.

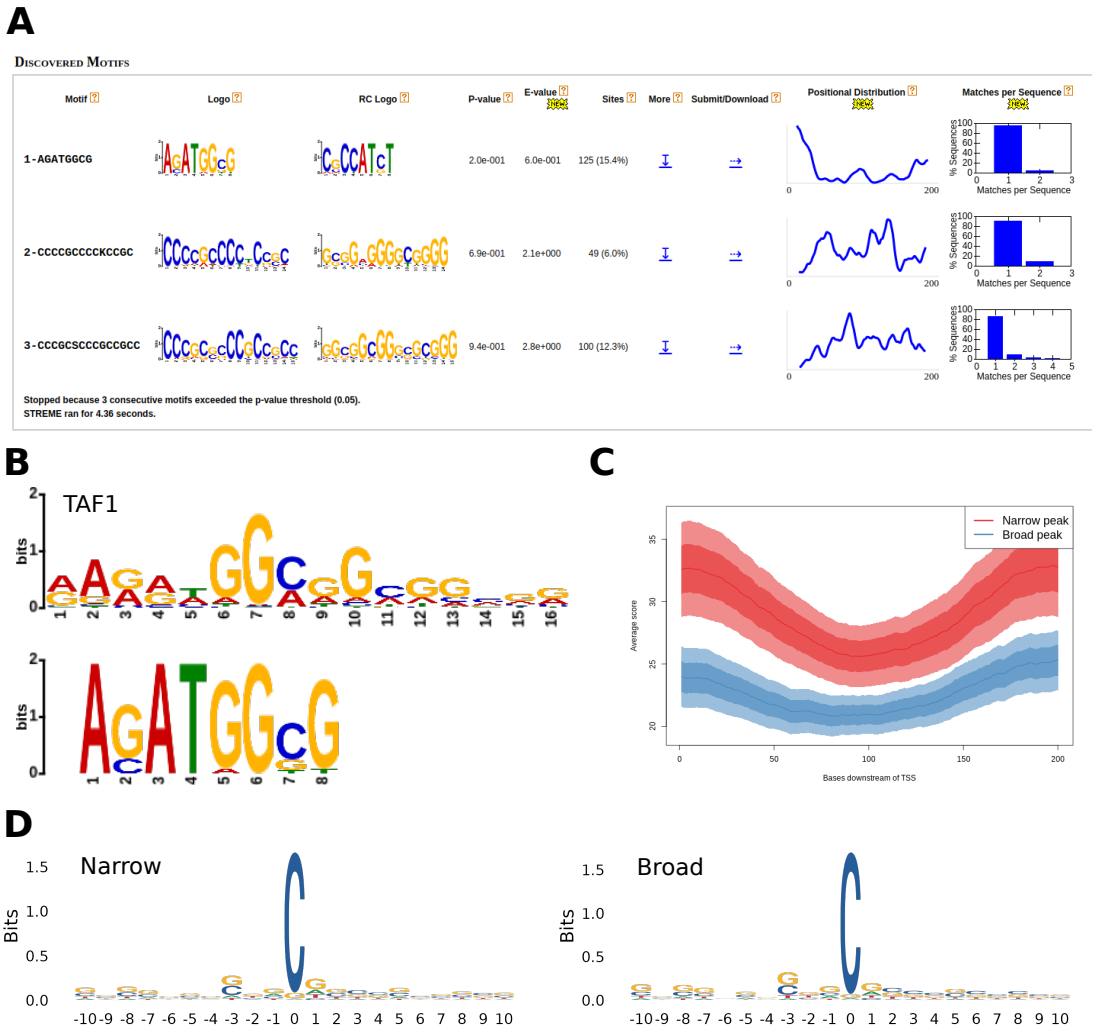

Supplementary Figure S4: Motifs identified in pause peaks from the control sample from the heat-shock data set [1] **A.** Motifs enriched in the 10% genes with narrowest pause peaks (smallest $\hat{\sigma}^2$) compared with the 10% of genes with broadest peaks (largest $\hat{\sigma}^2$) as identified by STREME [3]. **B.** The top candidate from STREME matches the binding motif of TAF1 [4]. **C.** TAF1 ChIP-seq signals from ENCODE [5] for narrow (red) and broad (blue) peaks downstream of the TSS. **D.** Sequences enriched at the site having the maximum PRO-seq read count in the pause peak (200 bp downstream of the TSS).

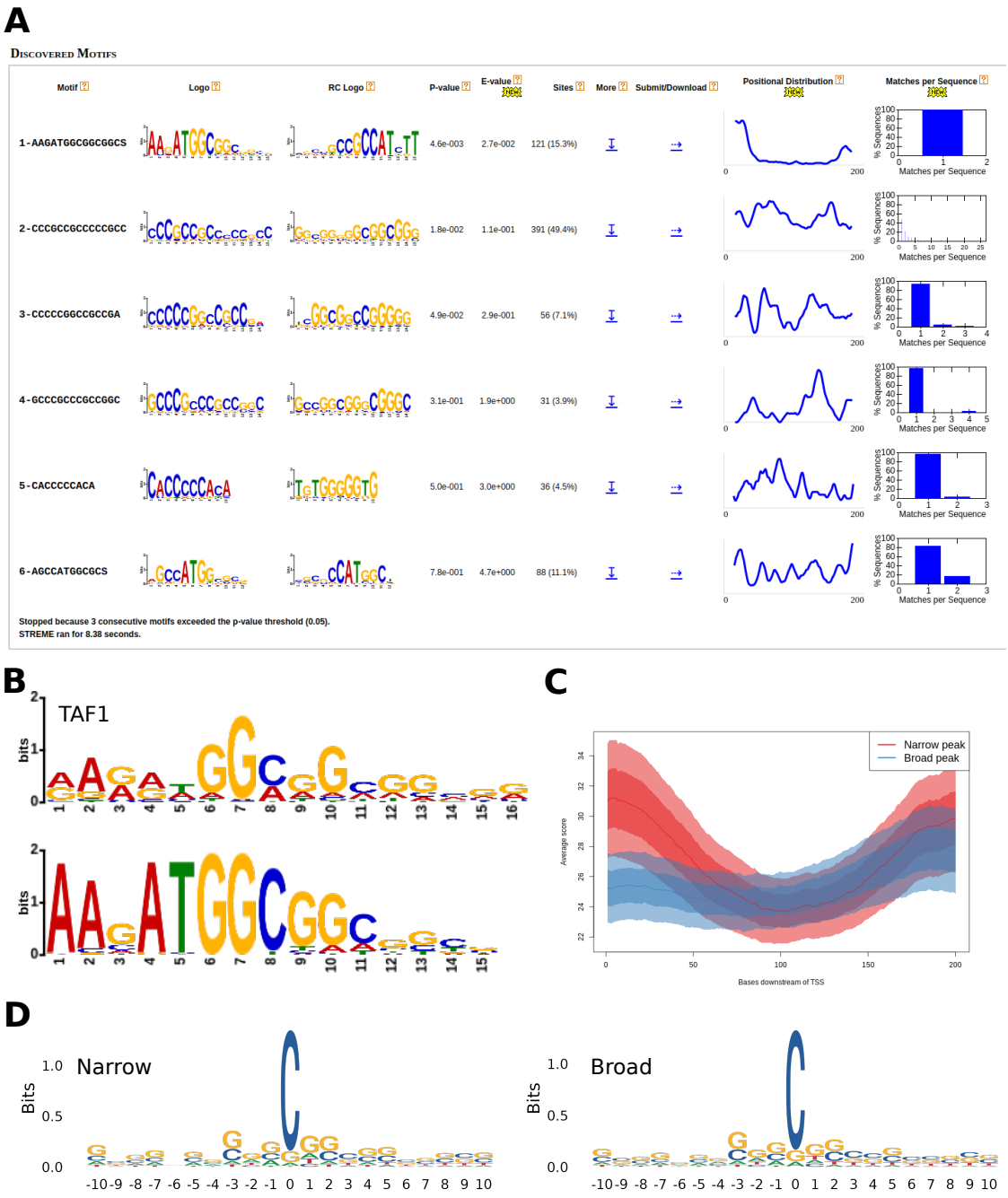

Supplementary Figure S5: Motifs identified in pause peaks from control sample from the celastrol data set [2] **A.** Motifs enriched in the 10% genes with narrowest pause peaks (smallest $\hat{\sigma}^2$) compared with the 10% of genes with broadest peaks (largest $\hat{\sigma}^2$) as identified by STREME [3]. **B.** The top candidate from STREME matches the binding motif of TAF1 [4]. **C.** TAF1 ChIP-seq signals from ENCODE [5] for narrow (red) and broad (blue) peaks downstream of the TSS. **D.** Sequences enriched at the site having the maximum PRO-seq read count in the pause peak (200 bp downstream of the TSS).

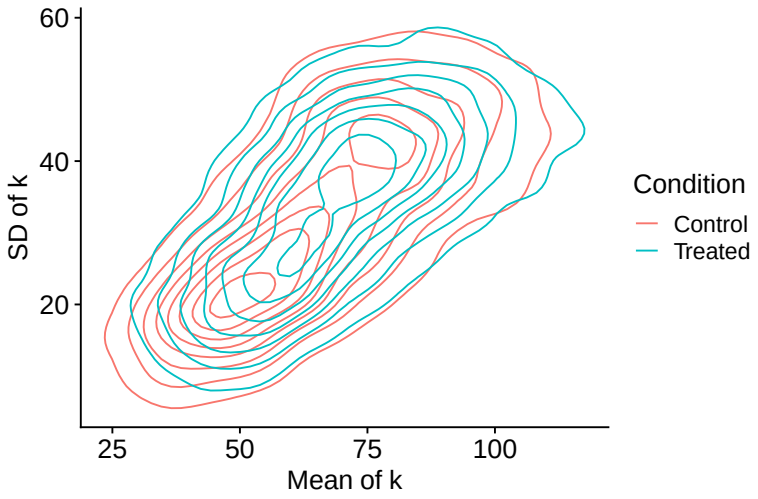

Supplementary Figure S6: Contour plot showing the distribution of estimated means (horizontal axis) and standard deviations (vertical axis) of the pause peak position k, under the Celastrol ("Treated") and Control conditions. Data from ref. [2]. Compare with **Fig. 3E**.

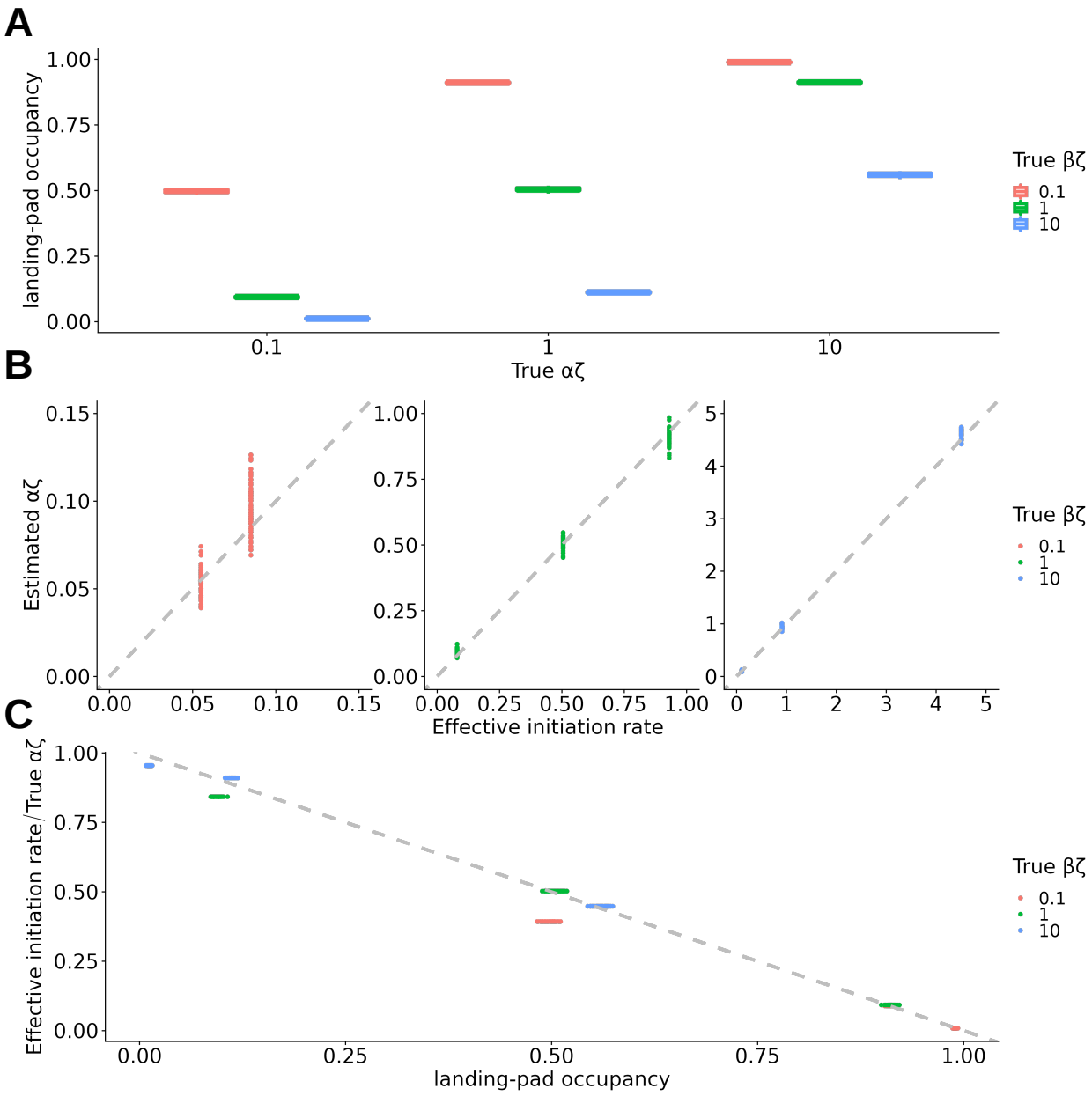

Supplementary Figure S7: Auxiliary data from simulations revealing prevalance of steric hindrance. **A.** Fraction of cells in which the "landing pad" (here, the first 50 bp) for a potential new initiation event is already occupied by an RNAP, for $\alpha\zeta \in \{0.1, 1, 10\}$ (left to right) and $\beta\zeta \in \{0.1, 1, 10\}$ (see key). **B.** Rates at which initiation rates successfully occur ("effective initiation rate") vs. estimates of $\alpha\zeta$, for true $\alpha\zeta \in \{0.1, 1, 10\}$ (left to right) and $\beta\zeta \in \{0.1, 1, 10\}$ (see key). The estimates of $\alpha\zeta$ are much closer to the effective initiation rates than to the true initiation rates. **C.** Landing-pad occupancy (as in panel **A**) vs. "correctness" of estimated $\alpha\zeta$, as measured by the ratio of the estimated value to the true value. The correctness decreases approximately linearly with the landing-pad occupancy.

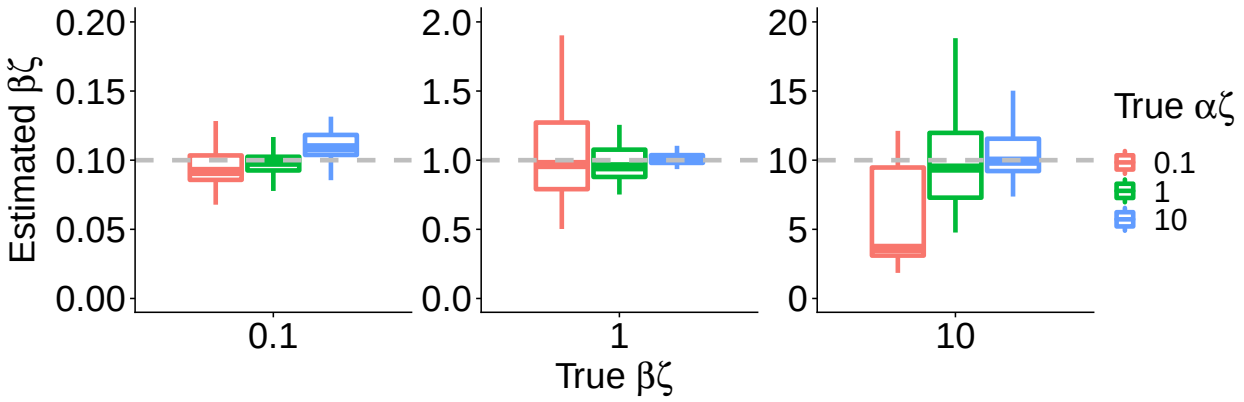

Supplementary Figure S8: Estimated values of $\beta\zeta$ under the steric hindrance model for simulated true values of $\beta\zeta \in \{0.1, 1.0, 10\}$ (left to right) and $\alpha\zeta \in \{0.1, 1, 10\}$ (see key). Estimates are close to the truth, except for the case of $\beta\zeta = 10$, $\alpha\zeta = 0.1$, for which the pause peak was poorly defined. As in previous plots, dashed lines indicate the ground truth; boxplots summarize 50 replicates of the simulation; box boundaries indicate 1st and 3rd quartiles, and horizontal line indicates median. A value of $\zeta = 2$ kb/min is assumed so that $\alpha\zeta$ and $\beta\zeta$ can be assumed to have units of events per minute. Pause sites are variable with a mean position of $k = 50$ bp and a standard deviation of 25 bp.

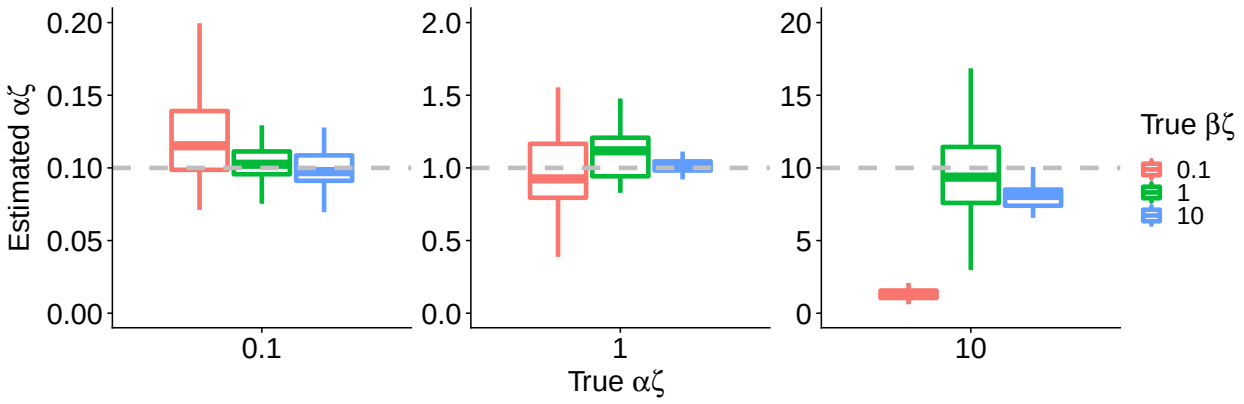

Supplementary Figure S9: Estimated values of $\alpha\zeta$ under the steric hindrance model, for $\alpha\zeta \in \{0.1, 1, 10\}$ (left to right) and $\beta\zeta \in \{0.1, 1, 10\}$ (see key). The poor estimate for $\alpha\zeta = 10, \beta\zeta = 0.1$ reflects underestimation of ϕ near the boundary of $\phi = 1$. As in previous plots, dashed lines indicate the ground truth; boxplots summarize 50 replicates of the simulation; box boundaries indicate 1st and 3rd quartiles, and horizontal line indicates median. A value of $\zeta = 2$ kb/min is assumed so that $\alpha\zeta$ and $\beta\zeta$ can be assumed to have units of events per minute. Pause sites are variable with a mean position of $k = 50$ bp and a standard deviation of 25 bp.

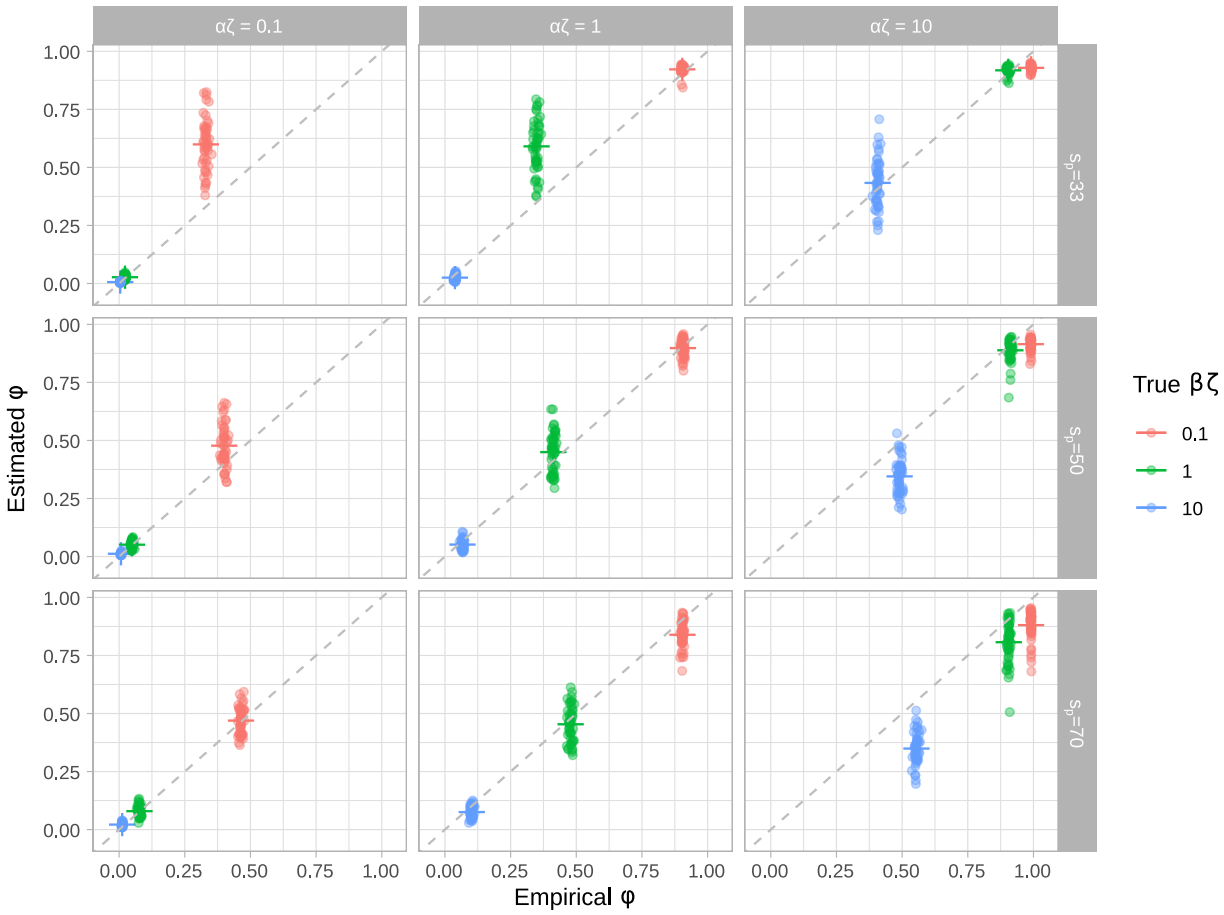

Supplementary Figure S10: Accuracy of estimated landing-pad occupancy ϕ under the steric hindrance model, for various values of $\alpha\zeta$ (columns), the spacing s_p between RNAPs (rows), and $\beta\zeta$ (see key). Scatter plots show the fraction of simulated cells for which the first 33, 50, or 70 bp (the "landing-pad") are occupied by an RNAP at steady state ("Empirical ϕ") vs. the fraction predicted to be occupied under the model ("Estimated ϕ") based on the simulated NRS data. 50 simulations were performed per parameter combination. Dashed line indicates $y = x$, and colored crosses represent the means of the corresponding points. A value of $\zeta = 2$ kb/min is assumed, so that $\alpha\zeta$ and $\beta\zeta$ are in events per minute.

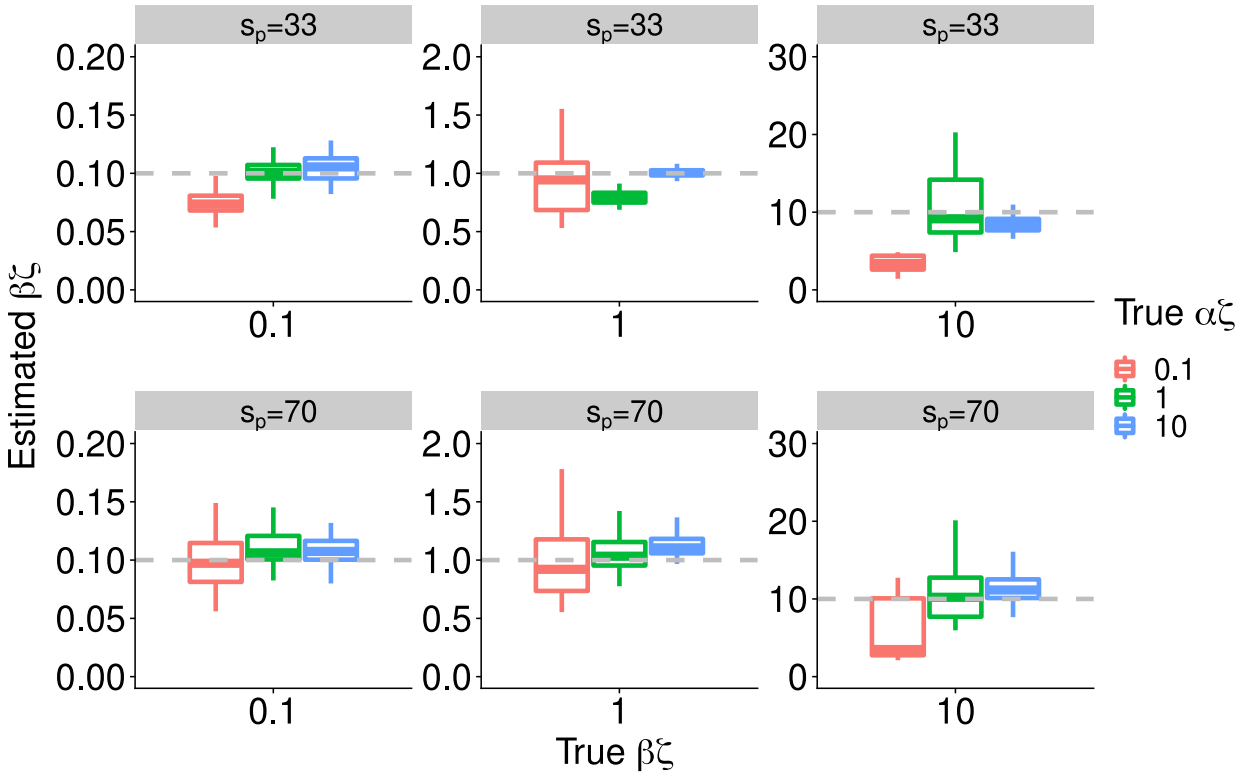

Supplementary Figure S11: Estimated values of $\beta\zeta$ under the steric hindrance model with alternative choices of the spacing parameter s_p (rows). Results are shown for simulated true values of $\beta\zeta \in \{0.1, 1.0, 10\}$ (left to right) and $\alpha\zeta \in \{0.1, 1, 10\}$ (see key). As in previous plots, dashed lines indicate the ground truth; boxplots summarize 50 replicates of the simulation; box boundaries indicate 1st and 3rd quartiles, and horizontal line indicates median. A value of $\zeta = 2$ kb/min is assumed so that $\alpha\zeta$ and $\beta\zeta$ can be assumed to have units of events per minute. Pause sites are variable with a mean position of $k = 50$ bp and a standard deviation of 25 bp.

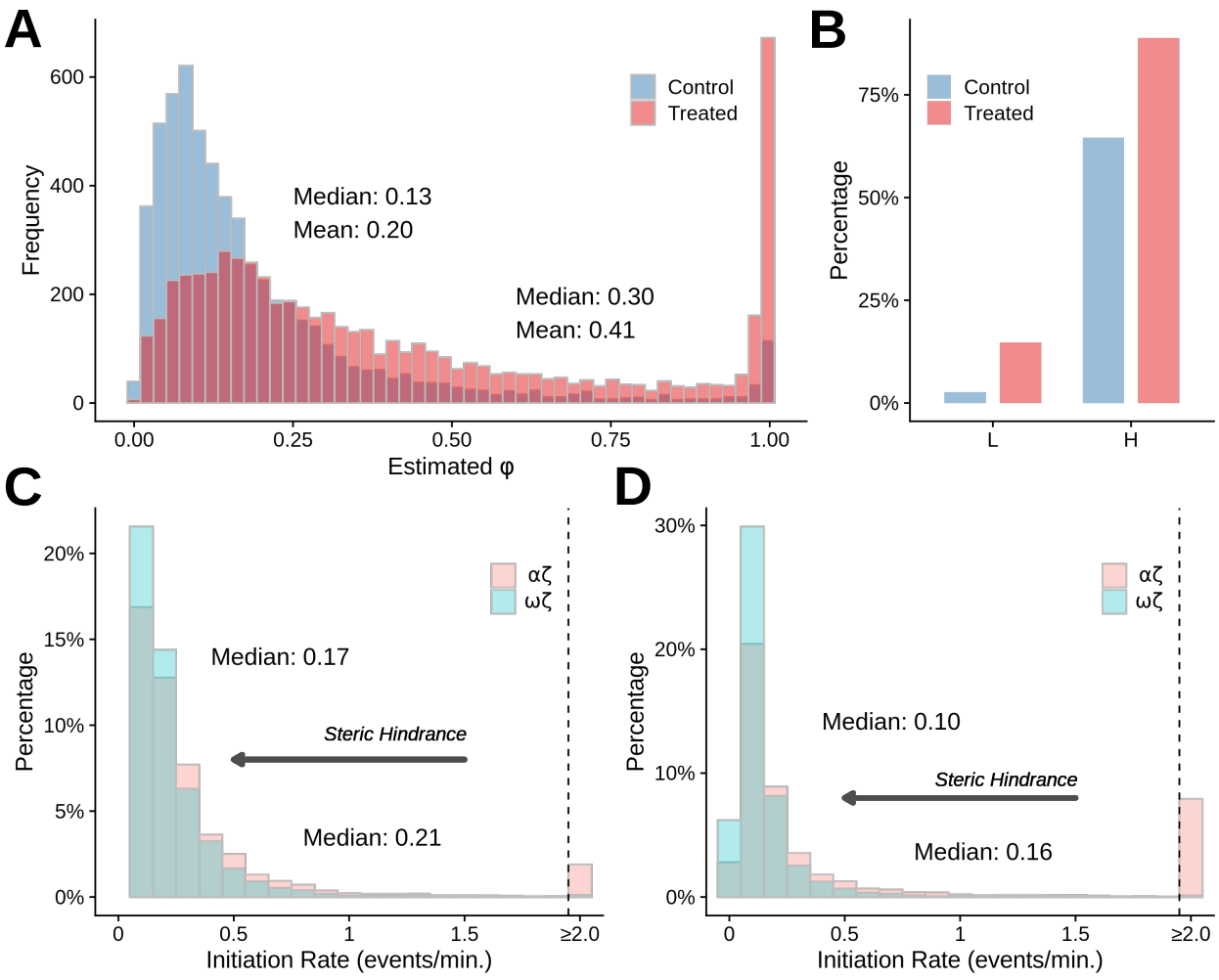

Supplementary Figure S12: **A.** Distribution of estimated ϕ for 5,964 robustly expressed genes in K562 cells before (Control) and after (Treated) treatment with celastrol under the low (L) calibration [2] (see **Methods** for details). **B.** Percentages of genes having fully occupied landing-pads ($\phi > 0.95$) before (Control) and after (Treated) treatment with celastrol, under the low (L) and high (H) calibrations. **C & D.** Distributions of scaled estimates of the "effective" ($\omega\zeta$) and "potential" ($\alpha\zeta$) rates of transcription initiation, in events per minute per cell, for the same genes. Panel **C** represents the NHS case and panel **D** represents the HS case. The x-axes are truncated to highlight the bulk of the distributions. Gray arrows indicate effects of steric hindrance.

References

[1] Vihervaara, A. *et al.* Transcriptional response to stress is pre-wired by promoter and enhancer architecture. *Nat Commun* **8**, 255 (2017).

[2] Dukler, N. *et al.* Nascent RNA sequencing reveals a dynamic global transcriptional response at genes and enhancers to the natural medicinal compound celastrol. *Genome Res* **27**, 1816–1829 (2017).

[3] Bailey, T. L. STREME: Accurate and versatile sequence motif discovery. *Bioinformatics* (2021).

[4] Gupta, S., Stamatoyannopoulos, J. A., Bailey, T. L. & Noble, W. S. Quantifying similarity between motifs. *Genome Biol* **8**, R24 (2007).

[5] Dunham, I. *et al.* An integrated encyclopedia of DNA elements in the human genome. *Nature* **489**, 57–74 (2012).